







Activation of lysophagy by a TBK1-SCF^{FBXO3}-TMEM192-TAX1BP1 axis in response to lysosomal damage

Received: 15 December 2023

Accepted: 14 January 2025

Published online: 28 January 2025



Na Yeon Park ^{1,2}, Doo Sin Jo³, Jae-Yoon Yang¹, Ji-Eun Bae ^{2,4}, Joon Bum Kim¹, Yong Hwan Kim¹, Seong Hyun Kim¹, Pansoo Kim³, Dong-Seok Lee ¹, Tamotsu Yoshimori⁵, Eun-Kyeong Jo ⁶, Eunbyul Yeom ^{1,4} ✉ & Dong-Hyung Cho ^{1,2,3} ✉

Lysophagy eliminates damaged lysosomes and is crucial to cellular homeostasis; however, its underlying mechanisms are not entirely understood. We screen a ubiquitination-related compound library and determine that the substrate recognition component of the SCF-type E3 ubiquitin ligase complex, SCF^{FBXO3} (FBXO3), which is a critical lysophagy regulator. Inhibition of FBXO3 reduces lysophagy and lysophagic flux in response to L-leucyl-L-leucine methyl ester (LLOMe). Furthermore, FBXO3 interacts with TMEM192, leading to its ubiquitination in LLOMe-treated cells. We also identify TAX1BP1 as a critical autophagic adaptor that recognizes ubiquitinated TMEM192 during lysophagy and find that TBK1 activation is crucial for lysophagy, as it phosphorylates FBXO3 in response to lysosomal damage. Knockout of FBXO3 significantly impairs lysophagy, and its reconstitution with a loss-of-function mutant (V221I) further confirms its essential role in lysophagy regulation. Collectively, our findings highlight the significance of the TBK1-FBXO3-TMEM192-TAX1BP1 axis in lysophagy and emphasize the critical role of FBXO3 in lysosomal integrity.

Lysosomes are organelles bound by a single membrane that play a pivotal role in cellular degradation and nutrient recycling. Mature lysosomes have an acidic internal pH (4.5–5.0), which is generated and maintained by a proton pumping v-type ATPase¹. This acidic condition optimally activates and stabilizes various lysosomal hydrolases². These unique characteristics regulate lysosomal catabolic functions³. The lysosomal membrane is composed of numerous membrane proteins, which highlights the critical role that lysosomes perform in various cellular functions, such as nutrient sensing, ion signaling, and lipid homeostasis^{4,5}. Lysosomal membrane proteins undergo extensive glycosylation to

protect against the acidic luminal environment and maintain lysosome integrity^{5–7}.

Lysosome dysregulation has been associated with various diseases, including lysosomal storage disorders, neurodegenerative diseases, diabetes, and cancer⁸. Thus, lysosomal integrity is crucial for cellular health and overall homeostasis. Lysosomotropic agents, such as L-leucyl-L-leucine methyl ester (LLOMe), induce lysosomal membrane permeabilization^{9–12} and release lysosomal contents into the cytosol, which increases cytosolic acidity and triggers apoptotic pathways via the released lysosomal proteases¹³. In response to partial injury, the endosomal sorting complex required for transport (ESCRT-III) machinery is

¹School of Life Sciences, BK21 FOUR KNU Creative BioResearch Group, Kyungpook National University, Daegu, South Korea. ²Organelle Institute, Kyungpook National University, Daegu, South Korea. ³ORGASIS Corp. 260, Suwon, South Korea. ⁴KNU G-LAMP Project Group, KNU Institute of Basic Sciences, College of Natural Sciences, Kyungpook National University, Daegu, South Korea. ⁵Department of Genetics, Graduate School of Medicine, Osaka University, Osaka, Japan. ⁶Department of Microbiology, Chungnam National University College of Medicine, Daejeon, South Korea. ✉e-mail: yeb@knu.ac.kr; dhcho@knu.ac.kr

recruited to the damaged lysosomal membrane for repair¹⁴, then the transcription factor EB (TFEB) is activated via dephosphorylation and translocated from the cytosol to the nucleus to enhance lysosomal gene expression to replace damaged lysosomes^{15,16}. However, in cases of severe injury, damaged lysosomes are subjected to lysosomal selective autophagy (i.e., lysophagy) for removal.

In selective autophagy, cargo is typically labeled via E3 ligases with ubiquitin, a small protein recognized by autophagy adaptor proteins, such as sequestosome 1 (SQSTM1/p62)¹⁷. During lysophagy, ruptured lysosomes are selectively labeled with galectins and ubiquitin⁹. Galectins, a conserved family of cytosolic lectins with carbohydrate recognition domains, exhibit a high affinity for β -galactoside glycoconjugates¹⁸. Since most lysosomal membrane proteins are glycosylated, their β -galactosides are exposed to the cytosol following lysosomal rupture and are recognized by galectins^{19–23}. Among the galectins, the galectin 3 (Gal3) has emerged as a widely used marker for lysosomal damage^{9,24}. Damaged lysosomes are also marked with ubiquitin. It was reported that some lysosomal membrane proteins are ubiquitinated as substrates in response to lysosomal damage, including lysosomal associated membrane protein 1 (LAMP1), LAMP2, and transmembrane protein 192 (TMEM192)²⁵. Several enzymes contribute to the ubiquitination of lysosomal membrane proteins during lysophagy. For example, LAMP2 is subject to ubiquitination as a substrate via the SCF E3 ligase complex SCF^{FBXO27}, which consists of S-phase-kinase-associated protein 1 (SKP1), Cullin-1 (CUL1), and F-box protein 27 (FBXO27) and the CUL4A-DDB1-WDFY1 complex^{25,26}. In addition, the ubiquitin-conjugating E2 enzyme (UBE2QL1) participates in the ubiquitination of LAMP1 by coordinating with lysophagy effectors²⁷. Autophagic adaptor proteins, such as SQSTM1, tax1 binding protein 1 (TAX1BP1), and calcium binding and coiled-coil domain 2 (CALCOCO2), then recognize ubiquitin on the lysosomal membrane and recruit autophagic machinery to facilitate lysophagy^{9,27–29}. Thus, the ruptured lysosomes are finally degraded by lysophagy.

The most well-established ubiquitin-dependent mechanism in selective autophagy is mitochondrial selective autophagy. As a mitophagy regulatory mechanism, PTEN-induced kinase 1 (PINK1) and E3 ligase Parkin participate in the ubiquitination of damaged mitochondrial membrane proteins. Upon mitochondrial damage, PINK1 is stabilized, accumulates on the mitochondrial membrane, and recruits cytosolic Parkin³⁰, which mediates the ubiquitination of mitochondrial outer membrane proteins, such as the voltage dependent anion channel 1 (VDAC1)³¹. Then, the adaptor proteins (e.g., SQSTM1, optineurin (OPTN) and CALCOCO2) recognize the ubiquitination and recruit autophagic machinery to degrade the mitochondria³². Therefore, in mitophagy, PINK1 and Parkin serves as a mitochondrial damage sensor kinase and downstream E3 ligase, respectively. Thus, the PINK1-Parkin-VDAC1-SQSTM1 axis is a well-documented scenario for mitophagy.

Although the significance of lysophagy in maintaining cellular homeostasis and cell fate is well established, the precise regulatory mechanisms coordinating sensor kinase-E3 ligase-membrane ubiquitination target-adaptor recruitment scenario remain unclear. Thus, we screened a ubiquitination-related compound library to identify lysophagy regulators. Our results propose a model in which the TBK1-FBXO3-TMEM192-TAX1BP1 axis orchestrates lysophagy by facilitating the ubiquitination of damaged lysosomal membranes.

Results

Inhibition of FBXO3 impairs clearance of Gal3 puncta and lysophagic flux

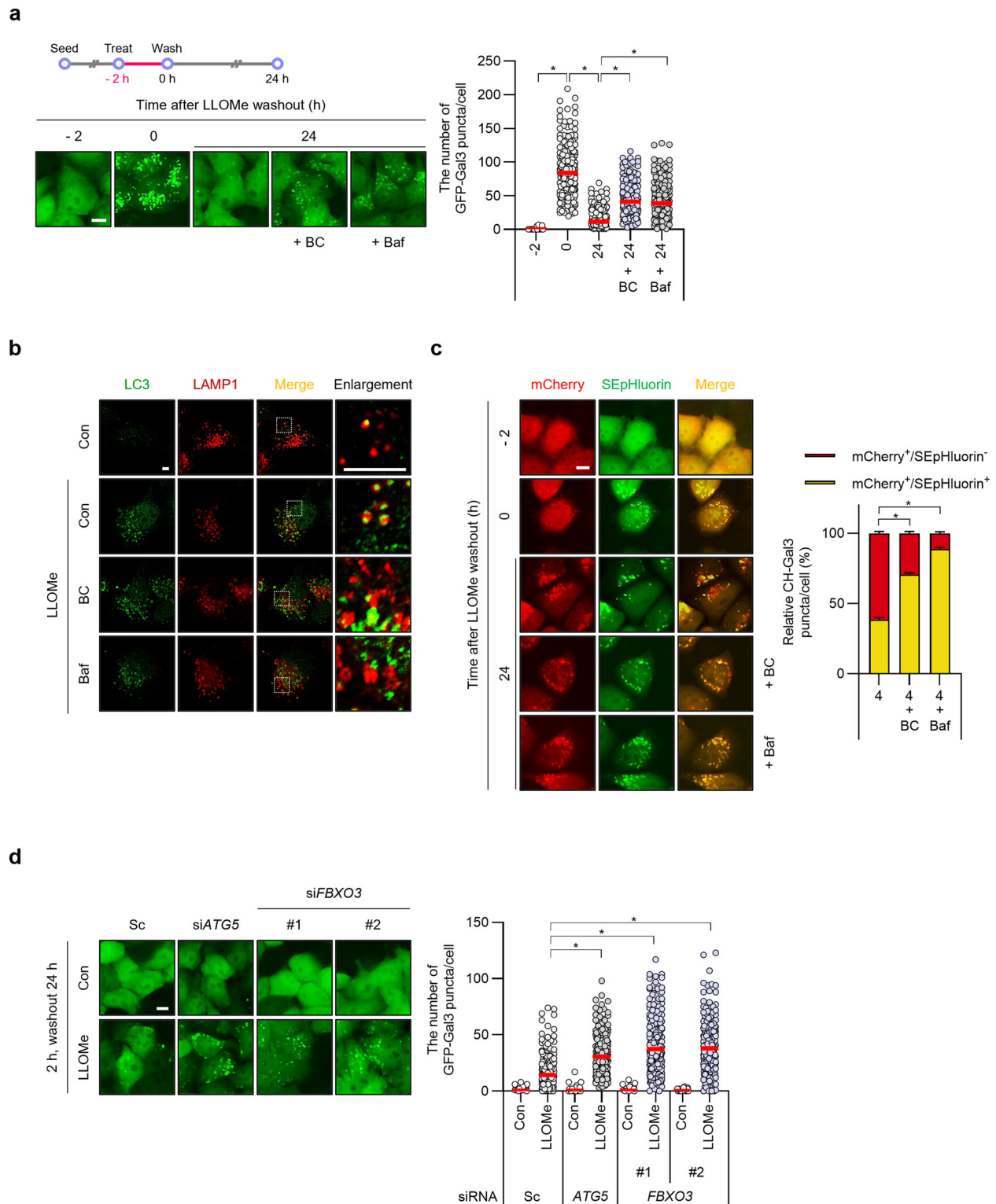
We developed a cell-based image screening system using enhanced green fluorescent protein (EGFP)-Gal3 in HepG2 cells (HepG2/GFP-Gal3 cells) and conducted a screening using a ubiquitination compound library in combination with a lysosomotropic agent, LLOMe to uncover lysophagy mechanisms. From the screening, we identified BC-1215 as the most potent lysophagy regulator (Supplementary Fig. 1;

Supplementary Tables 1, 2). To validate these findings, we subjected HepG2/GFP-Gal3 cells to cotreatment with LLOMe and bafilomycin A₁ (Baf), which blocks autophagosome-lysosome fusion. As demonstrated in Fig. 1a, BC-1215 significantly impeded the clearance of damaged lysosomes in the LLOMe-treated cells, which was similar to the Baf treatment; however, BC-1215 treatment alone at various concentrations did not affect GFP-Gal3 puncta formation (Fig. 1a; Supplementary Fig. 2a, b), indicating that BC-1215 specifically targets lysophagy in LLOMe-treated cells. Additionally, LLOMe-induced damage results in the partial encapsulation of lysosomes, labeled with LAMP1, within autophagosomes, as labeled with LC3. However, treatment with BC-1215 reduced this encapsulation, similar to the effects of Baf (Fig. 1b). As SEpHluorin is more pH-sensitive than EGFP, we established a lysophagy flux monitoring system using mCherry-SEpHluorin-Galectin 3 (CH-Gal3) in HepG2 cells (HepG2/CH-Gal3 cells). Consistently, the mCherry⁺/SEpHluorin⁻-Gal3 puncta decreased, whereas the mCherry⁺/SEpHluorin⁺-Gal3 puncta increased in cells treated with Baf or BC-1215 (Fig. 1c). Furthermore, LC3-II protein levels were higher in cells cotreated with LLOMe and either Baf or BC-1215 than those treated with each compound alone (Supplementary Fig. 3). BC-1215 is a highly selective inhibitor of FBXO3 that binds to the ApaG domain of FBXO3 and disrupts its interaction with substrates^{33,34}. To further investigate the role of FBXO3 in GFP-Gal3 puncta clearance regulation, we transfected HepG2/GFP-Gal3 cells with either scrambled siRNA or specific siRNA targeting *FBXO3* then treated them with LLOMe. The depletion of FBXO3 resulted in a marked decrease in the elimination of GFP-Gal3 puncta, comparable to other well-known lysophagy regulators including FBXO2, CUL4A, UBE2QL1^{26,27,35}, or the autophagy regulator autophagy-related 5 (ATG5) (Fig. 1d; Supplementary Figs. 4, 5). Taken together, these results indicate that the inhibition of FBXO3 hinders the clearance of damaged lysosomes and lysophagic flux in LLOMe-treated cells.

FBXO3 mediates ubiquitination of a lysosomal membrane protein, TMEM192 in response to lysosomal damage

To further elucidate the involvement of FBXO3 in lysophagy, we identified potential lysosomal membrane protein targets for ubiquitination in LLOMe-treated cells via immunoprecipitation assays. We found that FBXO3 did not directly interact with LAMP1 but that it exhibited binding affinity toward VAMP3 (Supplementary Fig. 6a, b). Despite the enhanced interaction between FBXO3 and VAMP3, VAMP3 ubiquitination was only marginally affected in LLOMe-treated cells (Supplementary Fig. 6c), suggesting that FBXO3 does not primarily mediate lysophagy through LAMP1 or VAMP3.

Next, our focus turned to TMEM192 as a potential target of FBXO3. As shown in Fig. 2, the interaction between FBXO3 and TMEM192 was further upregulated in response to LLOMe treatment (Fig. 2a–d). Remarkably, the ubiquitination of TMEM192 was significantly enhanced in LLOMe-treated cells compared to in untreated control cells (Supplementary Fig. 6d), which firmly established TMEM192 as a ubiquitinated target of FBXO3 in LLOMe-treated HepG2 cells. We also found that deletion of the F-box, SUKH, or ApaG domains of FBXO3 resulted in minor alterations in the interaction with TMEM192, with the F-box deletion showing a slight increase (Supplementary Fig. 6e, f). TMEM192 harbors multiple putative ubiquitination lysine residues, including K201, K211, K237, K246, and K254²⁵. To discern whether the lysine residues of TMEM192 underwent ubiquitination in response to LLOMe, we generated a TMEM192 mutant where all lysine candidates were substituted with arginine to impede ubiquitination. The mutant with substitutions at all five lysine sites exhibited reduced TMEM192 ubiquitination in LLOMe-treated cells (Fig. 2e). Importantly, both chemical and genetic inhibition of FBXO3 effectively suppressed TMEM192 ubiquitination in LLOMe-treated cells (Fig. 2f, g). The ubiquitination of TMEM192 modulated by FBXO3 was identified as K48-linked rather than K63-linked (Supplementary Fig. 6g). Furthermore, the depletion of TMEM192 significantly



impeded GFP-Gal3 puncta clearance that was induced by LLOMe treatment (Supplementary Fig. 7). Taken together, our findings suggest that FBXO3 orchestrates the ubiquitination of TMEM192 as a response to lysosomal damage.

SQSTM1 and TAX1BP1 interact with TMEM192 as autophagic adaptor in response to lysosomal damage

We next investigated the autophagic adaptors involved in the recognition of ubiquitinated TMEM192 in response to lysosomal damage.

Colocalization assay between TMEM192 and the adaptor protein NBR1 or OPTN revealed no substantial changes upon LLOMe treatment (Supplementary Fig. 8a, b). The interaction between NBR1 and TMEM192 was slightly reduced by LLOMe treatment and TMEM192 did not exhibit any significant binding to OPTN (Supplementary Fig. 8c, d). These results suggest that NBR1 and OPTN are unlikely to be the primary autophagic adaptors in TMEM192-mediated lysophagy. We further investigated other potential adaptors and found that the interaction between SQSTM1 or TAX1BP1 and TMEM192 was enhanced

Fig. 1 | Inhibition of FBXO3 reduces clearance of Gal3 puncta and lysophagic flux in HepG2 cells. **a** HepG2/GFP-Gal3 cells were cotreated with LLOMe (750 μ M), along with either bafilomycin A₁ (Baf) at 10 nM or BC-1215 (BC) at 50 μ M for 2 h. After the 2-h treatment, the cells were washed with fresh medium and further incubated with normal culture media containing either Baf or BC for 24 h. Subsequently, the number of punctate structures expressing GFP-Gal3 per cell was quantified. **b** HepG2 cells were cotreated with LLOMe, along with either Baf or BC for 2 h. Following treatment, the cells were washed with fresh medium and subsequently incubated with normal culture media containing either Baf or BC for an additional 24 h. Then, the cells were stained with anti-LAMP1 and anti-LC3 antibodies and imaged using confocal microscopy. Scale bar: 5 μ m. **c** HepG2/CH-Gal3 cells were cotreated with LLOMe and either Baf or BC-1215 for 2 h. After the 2-h treatment, LLOMe was removed, and the cells were incubated with normal cell media in the

presence of either Baf or BC-1215 for 24 h. The number of mCherry- and SepHluorin-double-positive-Gal3 puncta (mCherry⁺/SepHluorin⁺) or mCherry-positive/SepHluorin-negative-Gal3 puncta (mCherry⁺/SepHluorin⁻) per cell was counted. A total of 300 individual HepG2 cells were counted. **d** HepG2/GFP-Gal3 cells were transfected with either scrambled siRNA (Sc), siRNA targeting *FBXO3* (si*FBXO3*), or siRNA targeting *ATG5* (si*ATG5*) for a period of 48 h. Following transfection, the cells were treated with LLOMe for 2 h. After the 2-h treatment, the cells were washed and incubated with normal cell culture media for 24 h. The number of GFP-Gal3 puncta per cell was counted. Data in all panels are presented as the mean \pm SEM. Significance was calculated by two-tailed unpaired *t*-test ($p < 0.0001$). Data were obtained from at least three independent experiments, with each dot in the plot representing an individual HepG2 cell ($n = 300$). Scale bar: 10 μ m. Source data are provided as a Source Data file.

upon LLOMe treatment (Fig. 3a, b). Moreover, both SQSTM1 and TAX1BP1 exhibited significantly increased colocalization with TMEM192 WT, whereas colocalization with TMEM192 ubiquitin-defective mutant (MT) was reduced in LLOMe-treated cells (Fig. 3c, d), implicating their involvement as autophagic adaptors in TMEM192-mediated lysophagy. Additionally, GFP-Gal3 puncta clearance was impaired in cells expressing the TMEM192 mutant (Fig. 3e), and the knockdown of *SQSTM1* and *TAX1BP1* resulted in reduced GFP-Gal3 puncta clearance induced by LLOMe (Supplementary Fig. 9). Thus, either SQSTM1 or TAX1BP1 acts as autophagic adaptor that recognize ubiquitinated TMEM192 in response to lysosomal damage.

TBK1 activation in response to LLOMe mediates FBXO3 phosphorylation

To explore the upstream regulatory mechanisms governing FBXO3, we focused on TBK1 in LLOMe-mediated lysophagy using the TBK1 inhibitors MRT67307 and GSK8612. Treatment of inhibitors resulted in the reduced clearance of the GFP-Gal3 puncta induced by LLOMe (Fig. 4a). Moreover, LLOMe treatment highly enhanced phosphorylation of TBK1, which was abrogated by cotreatment with TBK1 inhibitors (Fig. 4b). Notably, the depletion of TBK1 also led to the decreased clearance of GFP-Gal3 puncta (Supplementary Fig. 10). Together, these results suggest that TBK1 activation is essential for efficient lysophagy.

Next, we investigated the possibility that TBK1 mediates FBXO3 activity as an upstream regulator. Coimmunoprecipitation studies demonstrated an interaction between TBK1 and FBXO3, which was further enhanced upon lysosomal damage (Fig. 4c, d). To investigate FBXO3 phosphorylation, we utilized a Phos-tagTM SDS-PAGE assay. Notably, FBXO3 underwent phosphorylation upon LLOMe treatment, which was diminished upon cotreatment with the TBK1 inhibitor (Fig. 4e). These observations indicate that TBK1 regulates FBXO3 phosphorylation in response to lysosomal damage.

Effect of TBK1-FBXO3-TMEM192-TAX1BP1 axis on LLOMe-induced lysophagy

Since TBK1 played a pivotal role in mediating the phosphorylation of FBXO3 in response to lysosomal damage (Fig. 4) and the FBXO3 facilitated the interaction with and subsequent ubiquitination of TMEM192 followed by the recruitment of the autophagic adaptor TAX1BP1 (Figs. 2, 3), we investigated the significance of the TBK1-FBXO3-TMEM192-TAX1BP1 axis in lysophagy. In response to LLOMe treatment, FBXO3 was found to localize to damaged lysosomes, as indicated by Gal3. Moreover, activated TBK1, detected by p-TBK1 staining, also colocalized with both FBXO3 and Galectin 3 on these damaged lysosomes, suggesting that TBK1 and FBXO3 can be activated on damaged lysosomes (Supplementary Fig. 11a). Remarkably, the enhanced interaction between FBXO3 and TMEM192 by LLOMe treatment was decreased by the FBXO3 or TBK1 inhibitor (Supplementary Fig. 11b, c). Correspondingly, the increased ubiquitination of TMEM192 triggered by LLOMe was diminished upon TBK1 inhibitor treatment (Fig. 5a). Furthermore, the recruitment of TAX1BP1 to

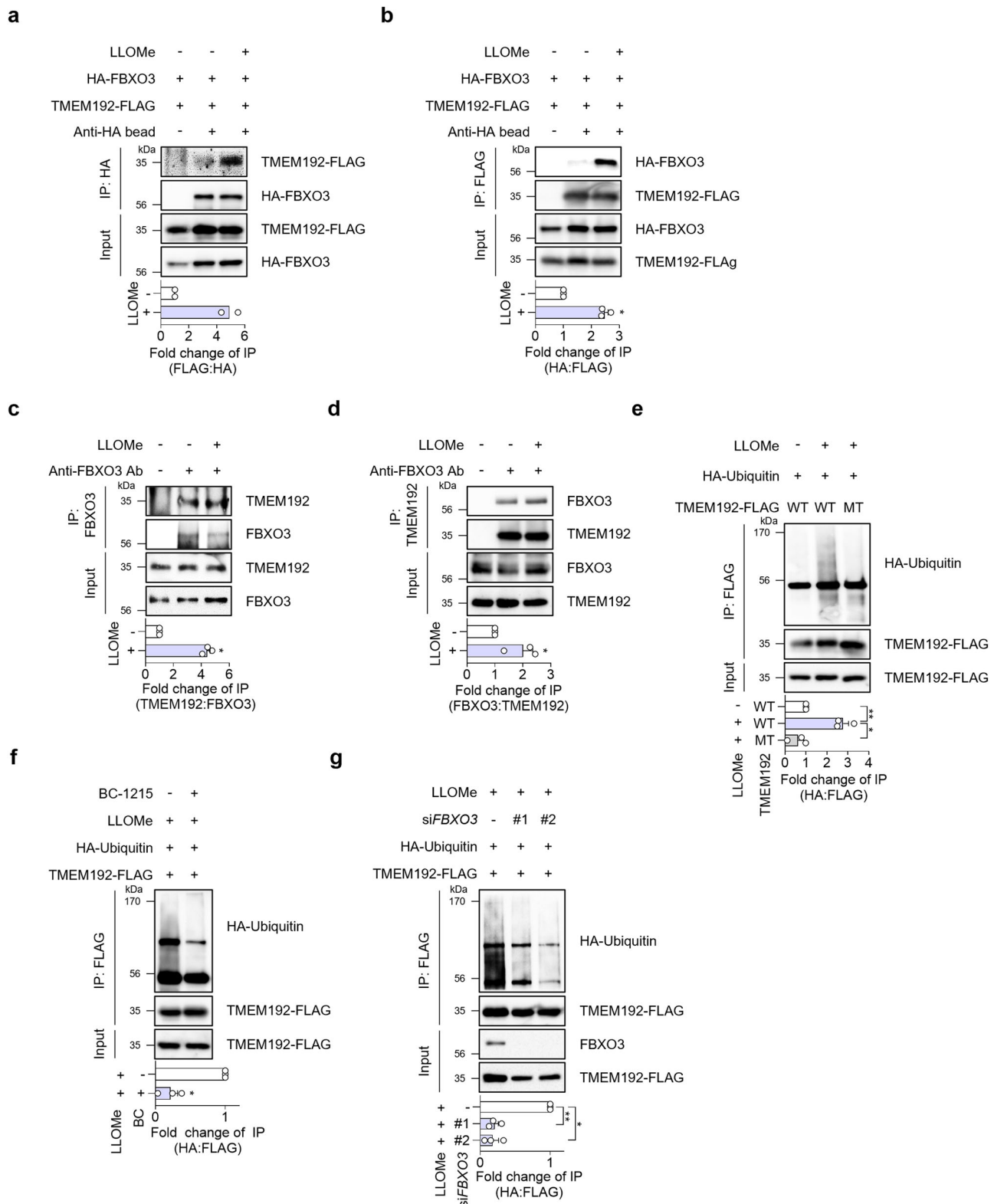
TMEM192 was reduced by both the FBXO3 and TBK1 inhibitors (Fig. 5b). We also investigated whether the axis influenced the recruitment of autophagic machinery. After LLOMe treatment, LC3 colocalized with TMEM192; however, the chemical inhibition of FBXO3 and TBK1 decreased the recruitment of LC3 to TMEM192 (Fig. 5c). Taken together, these findings strongly indicate the critical importance of the TBK1-FBXO3-TMEM192-TAX1BP1 axis in lysophagy regulation.

Association of FBXO3 with LLOMe-induced lysophagy in FBXO3 knockout HepG2 cells

We utilized CRISPR/Cas9 technology to generate FBXO3 knockout (KO) cell lines in HepG2 cells (Fig. 6a). We subjected FBXO3 wildtype (WT) and KO HepG2 cells transiently expressing GFP-Gal3 to LLOMe treatment. Our findings revealed decreased clearance of GFP-Gal3 puncta by LLOMe in FBXO3 KO cells compared to the WT cells (Fig. 6b). Additionally, the LLOMe-induced increase in TMEM192 ubiquitination was significantly lower in FBXO3 KO cells (Fig. 6c), which subsequently led to a diminished recruitment of TAX1BP1 to TMEM192 in FBXO3 KO cells compared to WT cells (Fig. 6d). These results indicate that FBXO3 KO disrupts the lysophagy by inhibiting the ubiquitination of TMEM192 and the recruitment of TAX1BP1. We additionally analyzed the human SNP database and identified a naturally occurring polymorphism in FBXO3 at Val221Ile (V221I) that represents a loss-of-function mutation^{33,36}. To assess the relevance of this FBXO3 mutant in lysophagy, we reintroduced either WT or FBXO3 V221I into FBXO3 KO cells and found that the delayed clearance of the Gal3 puncta observed in the KO cells was rescued by FBXO3 WT reconstitution; however, the clearance was still reduced when FBXO3 V221I was reintroduced (Fig. 6e). Furthermore, TMEM192 ubiquitination was restored in cells reconstituted with FBXO3 WT but remained impaired in FBXO3 V221I reconstituted cells (Fig. 6f). Collectively, these results further support the critical role of FBXO3 in the degradation of damaged lysosomes.

Association of TBK1-FBXO3-TMEM192-TAX1BP1 axis with LLOMe-induced lysophagy in *Drosophila* model

To examine lysophagy activity in the *Drosophila* model system, we generated a pUAST-mCherry-SEPfluorin-Gal3 transgenic fly line. This reporter system can be used to monitor lysophagy quality control, which changes its fluorescence signals as lysophagy progresses. mCherry-SEPfluorin-Gal3 was overexpressed using the *Dcg-Gal4* to drive in the larval fat body. To induce lysophagy, third-instar stage larvae were fed for 2 h with LLOMe treated fly food and transferred to normal fly food vial for each time period for (4 h and 8 h) or dissected immediately (0 h after LLOMe treatment). After LLOMe treatment for 2 h, mCherry- and SEPfluorin-double positive Gal3 puncta (mCherry⁺/SEPfluorin⁺) were observed. 4 h after transferred to normal food, mCherry⁺/SEPfluorin⁻ Gal3 puncta were increased, and those puncta almost disappeared after 8 h (Supplementary Fig. 12). To test the effect of inhibitors (i.e., BC-1215, GSK8612 and Baf), the larvae were cotreated with LLOMe for 2 h, and transferred to only inhibitors-treated food for



next 4 h. Consistent with in-vitro data, cotreatment of BC-1215, GSK8612 or Baf with LLOMe showed decrease of mCherry⁺/SEpHluorin⁺ Gal3 puncta in larva fat body. The ratio of mCherry⁺/SEpHluorin⁺ and mCherry⁺/SEpHluorin⁺ Gal3 puncta were counted and quantified (Fig. 7a). These results suggest that BC-1215, GSK8612 and Baf also downregulate clearance of Gal3 puncta induced by LLOMe in *Drosophila* in vivo model.

To investigate whether lysophagy induced by LLOMe is activated by FBXO3 also in *Drosophila*, we utilized *UAS-Slmb-RNAi* to knockdown *Slmb*, a homolog of F-box proteins, employing the fat body driver *Dcg-Gal4*. The larval fat body was costained with anti-ubiquitin and anti-LAMP1 antibodies. In comparison to control flies subjected to LLOMe treatment, where ubiquitin and LAMP1 exhibited partial colocalization, *Slmb* knockdown resulted in a significant

Fig. 2 | FBXO3 interacts with TMEM192 and mediates ubiquitination of TMEM192 in LLOMe-treated HepG2 cells. **a, b** HepG2 cells transiently expressing both HA-FBXO3 and TMEM192-FLAG were treated with LLOMe (750 μ M) for 2 h and immunoprecipitated with agarose beads-conjugated anti-HA or anti-FLAG antibodies. The immunoprecipitates were analyzed by western blotting. Data in panel **a** are presented as the mean ($n = 2$), and data in panel **b** are presented as the mean \pm SEM ($n = 3$, $*p = 0.0002$). **c, d** HepG2 cell lysates treated with LLOMe (750 μ M) were immunoprecipitated using either anti-FBXO3 or anti-TMEM192 antibodies. Then, the immune complexes were analyzed by western blotting. Data in panel **c** are presented as the mean \pm SEM ($n = 3$, $*p < 0.0001$), and data in panel **d** are presented as the mean \pm SEM ($n = 3$, $*p = 0.0438$). **e** HepG2 cells expressing TMEM192-FLAG wild type (WT) or a mutant (TMEM192 K201,211,237,246,254R) along with HA-ubiquitin were treated with LLOMe for 2 h. And then, the cells were subjected to immunoprecipitation using agarose-conjugated anti-FLAG antibody. The immunoprecipitates were

analyzed by western blotting. Data are presented as the mean \pm SEM ($n = 3$, $*p = 0.0044$, $**p = 0.0023$). **f** HepG2 cells overexpressing both HA-ubiquitin and TMEM192-FLAG were pretreated with BC-1215, and then cotreated with LLOMe for an additional 2 h. Subsequently, the cells were immunoprecipitated using anti-FLAG antibody conjugated to agarose beads. The immunoprecipitates were further analyzed by western blotting. Data are presented as the mean \pm SEM ($n = 3$, $*p = 0.0015$). **g** HepG2 cells were transfected with either scrambled siRNA or siRNA targeting FBXO3 siRNA in combination with HA-ubiquitin and TMEM192-FLAG for 72 h. After 72 h, the cells were treated with LLOMe for 2 h and subjected to immunoprecipitation using agarose-conjugated anti-FLAG antibody. The immune complexes were analyzed by western blotting. Data are presented as the mean \pm SEM ($n = 3$, $*p = 0.0005$, $**p = 0.0001$). All experiments were replicated three times except **a** (twice replicates). Two-tailed unpaired *t*-test were used to analyze the data. Source data are provided as a Source Data file.

reduction in the colocalization of LAMP1 and ubiquitin (Fig. 7b). This suggests that Slmb mediates lysophagy induced by LLOMe. Collectively, these findings provide compelling evidence that the FBXO3-TMEM192 axis plays a crucial role in LLOMe-induced lysophagy in *Drosophila*.

Discussion

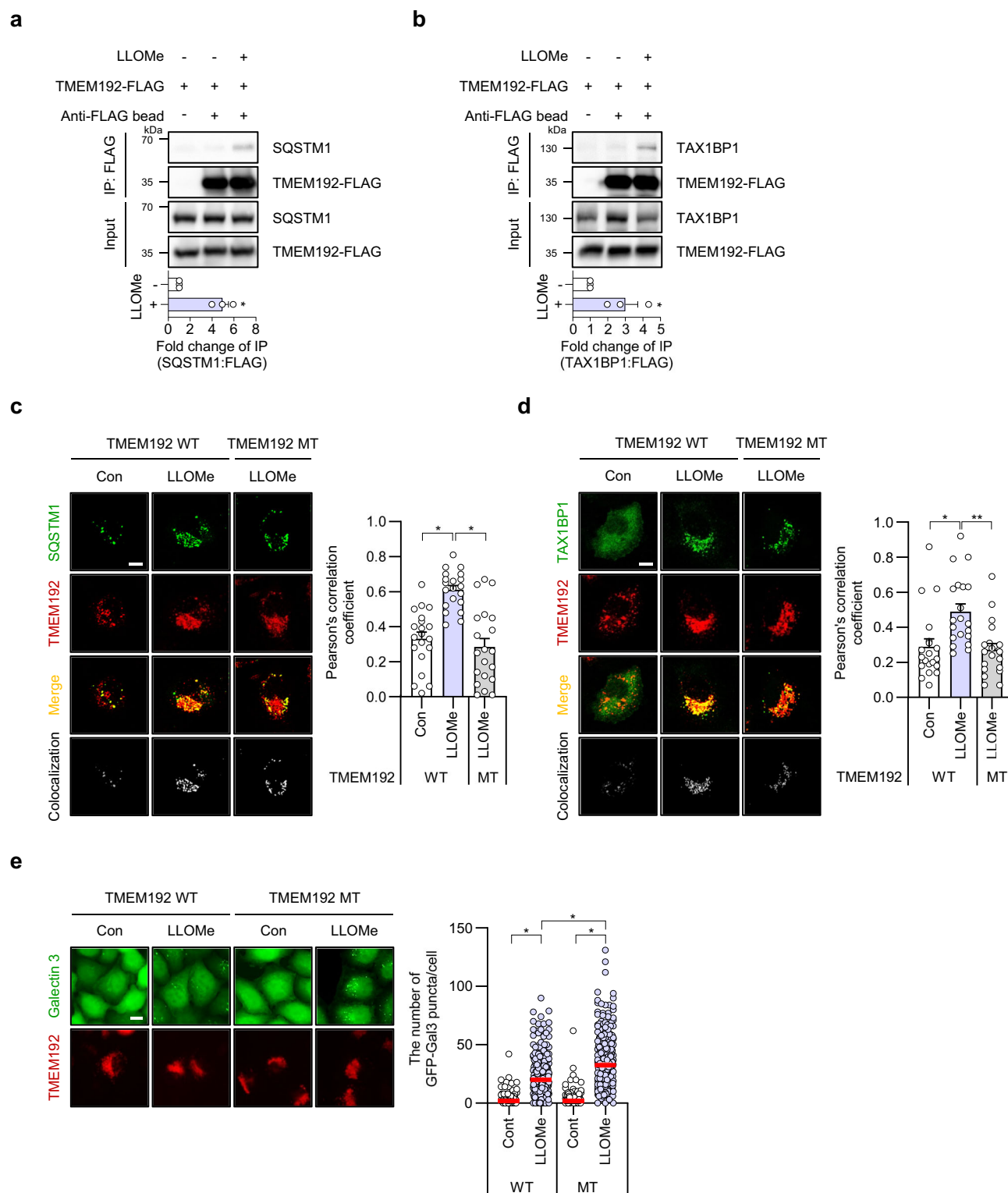
Maintaining lysosomal integrity is vital for cellular homeostasis and physiological functions. This integrity is tightly controlled by biogenesis, repair and degradation. Upon lysosomal injury, TFEB and ESCRT-III complex are activated to replace damaged lysosomes and repair lysosomal membrane. In cases of severe damage, ruptured lysosomes are eliminated through lysophagy. However, the precise regulatory mechanisms governing lysophagy are still not fully understood. A scenario of damage sensor kinase-E3 ligase-membrane protein ubiquitination-adaptor protein recruitment is well documented in mitophagy. In this process, PINK1 kinase recognizes mitochondrial damage and recruits an E3 ligase parkin, resulting in polyubiquitination of some mitochondrial membrane proteins, including VDAC1 and recruitment autophagy adaptor proteins such as SQSTM1. However, a cascade scenario, similar to PINK1-Parkin-VDAC1-SQSTM1, remains uncharacterized in lysophagy. In our study, we conducted a screening of ubiquitination-related compounds and discovered a regulatory mechanism of lysophagy, TBK1-FBXO3-TMEM192-TAX1BP1 axis scenario (Fig. 8). This lysophagy pathway is similar to mitophagy. Our findings emphasize the pivotal role of this axis in the degradation of ruptured lysosomes.

TMEM192 has been widely used to purify lysosomes due to its superior localization to lysosomes compared to other proteins^{28,37}. Notably, a previous study showed TMEM192 as a potential ubiquitinated transmembrane protein in response to lysosomal damage, with specific lysine residues²⁵. Protein structure topology has shown that both the N-terminus and C-terminus tails of TMEM192 are situated on the cytosolic side of the membrane³⁸. The implicated 5 lysine residues (201, 211, 237, 246, and 254) are positioned on the C-terminus of TMEM192. To uncover the critical polyubiquitin lysine residues involved in lysophagy, we conducted point mutagenesis, replacing each lysine with arginine to prevent ubiquitination. Notably, when all the lysine residues were mutated simultaneously, TMEM192 ubiquitination was entirely halted (Fig. 2e). From these results, it becomes evident that ubiquitination of TMEM192, as part of the lysophagy process, relies on multiple lysine residues. In addition to TMEM192, several lysosomal membrane proteins, such as LAMP1 and LAMP2, are also implicated as ubiquitination targets during lysophagy. Thus, these findings underscore the complexity and redundancy of the ubiquitination process, highlighting its crucial role in recognition and degradation of damaged lysosomes.

Recently, organelle membrane rupture has been elucidated as a stress factor that causes the release of cytotoxic contents, such as acidic lysosomal luminal compartments, and cell death¹². This makes

the ability to recognize membrane damage critical for cellular homeostasis. It was demonstrated that TBK1 plays an essential role as a membrane damage sensor kinase³⁹. During adenovirus infection, adenovirus enters the cell through endocytosis and reaches the cytosol by disrupting the endosomal membrane⁴⁰. Then, TBK1 is activated via phosphorylation at Ser172 and accumulates at the penetration site of the endosome to activate the selective autophagy of the invading pathogen (i.e., xenophagy)³⁹. Gal8 primarily recognizes pathogen-induced endosomal rupture and is critical in the local activation of TBK1⁴¹. It was reported that TBK1 is also highly associated with lysophagy. In response to lysosomal damage, activated TBK1 accumulates on ruptured lysosomes and the inhibition of TBK1 reduces lysophagic flux²⁸. Thus far, studies on TBK1 functions have been focused on its regulation of adaptor proteins during autophagy; however, recent reports have demonstrated that TBK1 is the upstream sensor kinase for membrane damage^{39–41}. Although the mechanism by which TBK1 senses signals from damaged lysosomes remains unclear, our study has identified TBK1 as a kinase that acts as a sensor of lysosomal damage and recruits FBXO3 (Fig. 4; Supplementary Fig. 11). As a kinase, TBK1 regulates FBXO3 activity via phosphorylation and FBXO3-mediated lysophagic flux. Based on the *in silico* analysis, we identified several potential phosphorylation sites on FBXO3, including Ser26, Ser166, Ser356, and Thr82. Therefore, further analysis to identify TBK1-dependent phosphorylated sites on FBXO3 is needed to understand the underlying mechanisms of lysophagy.

The F-box protein has a pivotal role in recognizing specific substrates^{42,43}. Only a few of them including FBXO27, FBXO2 and FBXO6 have been suggested as lysophagy regulators^{25,35}. These F-box proteins are markedly characterized with the ability to bind specifically glycoproteins modified with high-mannose-N-glycans, enable to recognize damaged lysosomes. Nevertheless, considering that over 70 F-box proteins are activated upon various stimuli, other F-box proteins also could become potential lysophagy regulators. Among them, we highly proposed that FBXO3, which structurally lacks a glycoprotein binding domain^{36,44}, acts as a crucial lysophagy regulator. While some substrates of these F-box proteins, such as LAMP1, are modified with N-glycans^{45,46}, TMEM192, despite bioinformatics predictions indicating two consensus sites for N-glycosylation, has not been shown to undergo N-Glycan modification in murine model⁴⁷. These findings lead us to hypothesize that FBXO3-mediated ubiquitination of TMEM192 may not depend on glycan modifications, unlike FBXO27. Nonetheless, considering the complexity of glycan modification in humans, further research is necessary to elucidate the relationship between TMEM192 modification and its ubiquitination. According to Human SNP database analysis, FBXO3 has non-synonymous C/T polymorphism, naturally occurring mutation in Val221Ile (V221I). The FBXO3 V221I variant, a loss of function, strikingly reduces the ability in substrate polyubiquitination³³. This loss of function mutation also reduced



lysophagy flux and ubiquitination of lysosomal membrane protein compared to WT upon lysosomal rupture, suggesting that FBXO3 is critical regulator in TMEM192-mediated lysophagy (Fig. 6).

Drosophila has its own set of F-box proteins, including Slmb (also known as β -TrCP), one of the most well-known F-box proteins. Slmb is essentially conserved component of Skp-Cullin-F-box (SCF) E3 ubiquitin ligase complex, and it plays a crucial role in regulating protein degradation through the ubiquitin-proteasome pathway in *Drosophila*⁴⁸. Several evidence demonstrate that *Drosophila* Slmb contributes in a variety of cellular processes regulating multiple

signaling pathways such as Wnt-TCF signaling pathway and Hedgehog signaling pathway⁴⁹. Recently, Slmb has been identified as a tumor suppressor gene which negatively regulates Hippo signaling, suggesting its essential role in development and organ growth⁵⁰. Here, we revealed for that Slmb is involved in lysophagy quality control in *Drosophila* model system. To study lysophagy in vivo, we generated mCherry-SEPhluorin-Gal3 transgenic reporter *Drosophila* line. *Drosophila* is an excellent system for monitoring changes of lysophagy activity in vivo due to its simple tissue structures and ease of dissection. Further research using these approaches in animal

Fig. 3 | TMEM192 interacts with SQSTM1 and TAX1BP1 as autophagic adaptors in response to lysosomal damage. **a, b** HepG2 cells expressing TMEM192-FLAG were treated with LLOMe (750 μ M, 2 h) and immunoprecipitated with an anti-FLAG antibody conjugated with agarose beads. Then, the cells were analyzed by western blotting. Data in the panel **a** are presented as the mean \pm SEM, with each dot in the plot representing independent replicates of the experiment ($n = 3$, $*p = 0.0021$). Data in the panel **b** are presented as the mean \pm SEM, with each dot in the plot representing independent replicates of the experiment ($n = 3$, $*p = 0.0452$). **c** HepG2 cells transiently expressing pEGFP-SQSTM1 in combination with TMEM192-FLAG wild type (WT) or ubiquitination-defective mutant (MT) were treated with LLOMe. The cells were stained with an anti-FLAG antibody and imaged using confocal microscopy. The colocalization extent of TMEM192 with SQSTM1 was analyzed using Pearson's correlation coefficients. Data are presented as the mean \pm SEM ($n = 20$, $*p < 0.0001$). **d** HepG2 cells were transiently transfected with

pTAX1BP1-EGFP in combination with TMEM192-FLAG WT or MT and then treated with LLOMe. Following treatment, the cells were stained with an anti-FLAG antibody and imaged using confocal microscopy. The degree of colocalization between TMEM192 and TAX1BP1 was quantified using Pearson's correlation coefficients. Data are presented as the mean \pm SEM ($n = 20$, $*p = 0.0025$, $**p = 0.0004$). **e** HepG2/GFP-Gal3 cells transiently expressing TMEM192-FLAG WT or MT and treated with LLOMe for 2 h. After treatment, cells were washed and incubated with fresh culture medium for an additional 24 h. Then, the cells were stained with an anti-FLAG antibody and imaged using fluorescence microscopy. The number of GFP-Gal3 puncta per cell expressing TMEM192-FLAG WT or MT was counted. Data are presented as the mean \pm SEM ($n = 300$, $*p < 0.0001$). Scale bar: 10 μ m. All experiments were replicated three times. Each dot in the plot **c**, **d**, and **e** represents an individual HepG2 cell. Two-tailed unpaired *t*-test were used to analyzed all the data. Source data are provided as a Source Data file.

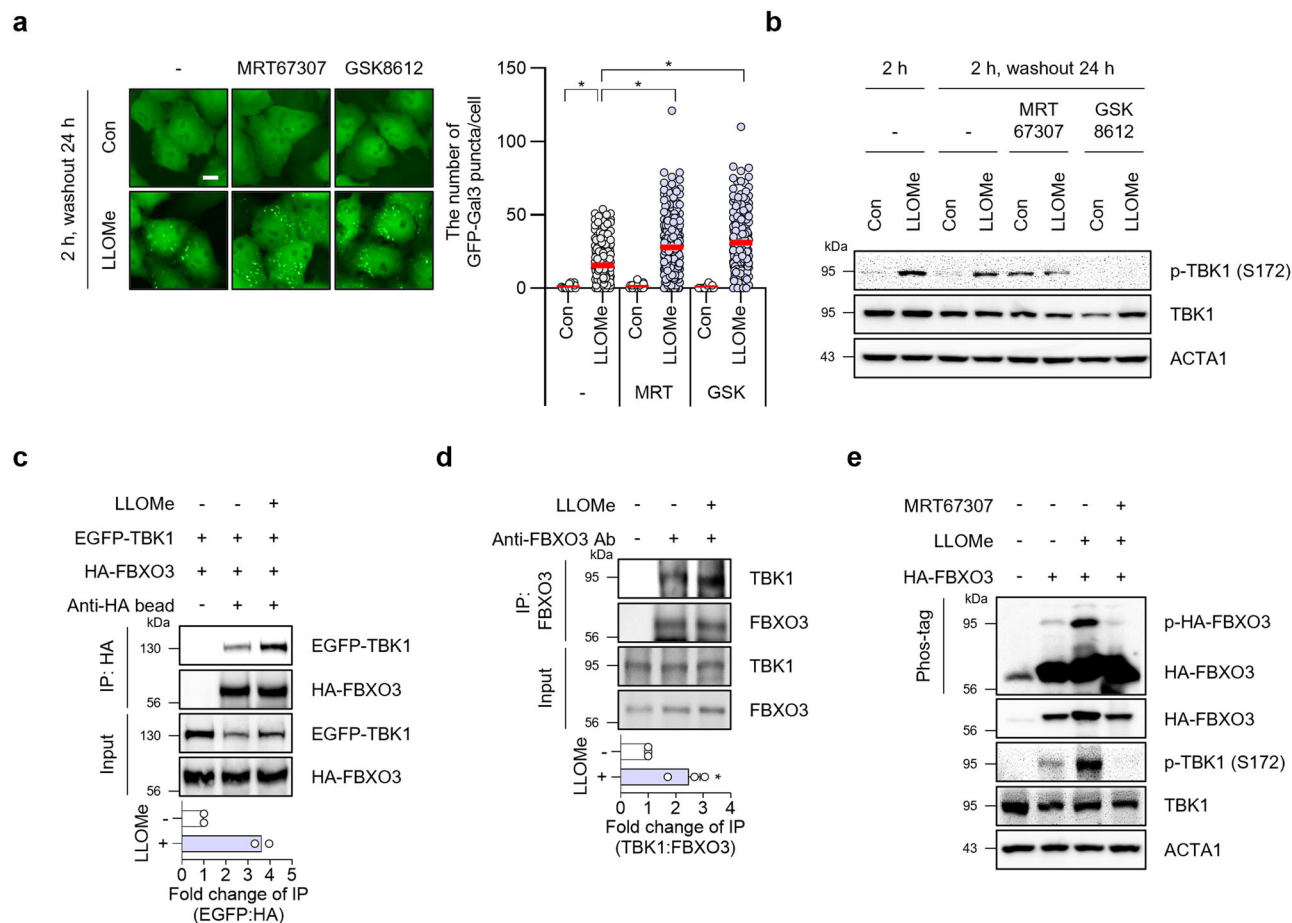


Fig. 4 | TBK1 is activated and mediates phosphorylation of FBXO3 in LLOMe-treated HepG2 cells. **a, b** HepG2/GFP-Gal3 cells were treated with either MRT67307 (2 μ M) or GSK8612 (10 μ M) in combination with LLOMe (750 μ M). After the 2-h treatment, LLOMe was washed out with normal cell culture media, and the cells were further incubated with either MRT67307 or GSK8612 for 24 h. The number of GFP-Gal3 puncta was quantified, and the cells were further analyzed by western blotting using the indicated antibodies. Data are presented as the mean \pm SEM, with each dot in the plot representing an individual HepG2 cell ($n = 300$, $*p < 0.0001$). Scale bar: 10 μ m. **c** HepG2 cells transiently expressing both GFP-TBK1 and HA-FBXO3 were treated with LLOMe. Subsequently, the cells were subjected to immunoprecipitation using an anti-HA antibody conjugated with agarose beads. The immunoprecipitates were further analyzed by western blotting

using the indicated antibodies. Data in all panels are presented as the mean ($n = 2$). **d** HepG2 cells were treated with LLOMe and subsequently lysed. The cell lysates were subjected to immunoprecipitation using an anti-FBXO3 antibody. Then, the immunoprecipitates were analyzed by western blotting using the indicated antibodies. Data are presented as the mean \pm SEM, with each dot in the plot representing independent triplicate replicates of the experiment ($n = 3$, $*p = 0.0212$). **e** HepG2 cells overexpressing either HA or HA-FBXO3 were pretreated with MRT67307 (2 μ M) for 2 h, followed by cotreatment with LLOMe. The cells were then subjected to analysis by Phos-tagTM SDS-PAGE and western blotting using the indicated antibodies. All experiments were replicated three times except c (twice replicates). Two-tailed unpaired *t*-test were used to analyzed all the data. Source data are provided as a Source Data file.

models could investigate the intricate molecular mechanisms underlying lysophagy, contributing significantly to developing targeted interventions and therapies for lysophagy-associated pathologies and disorders.

In conclusion, this study provides valuable insights into the molecular pathways that safeguard lysosomal integrity and cellular health and offers potential targets for therapeutic disease interventions associated with impaired lysophagy and lysosomal dysfunction.

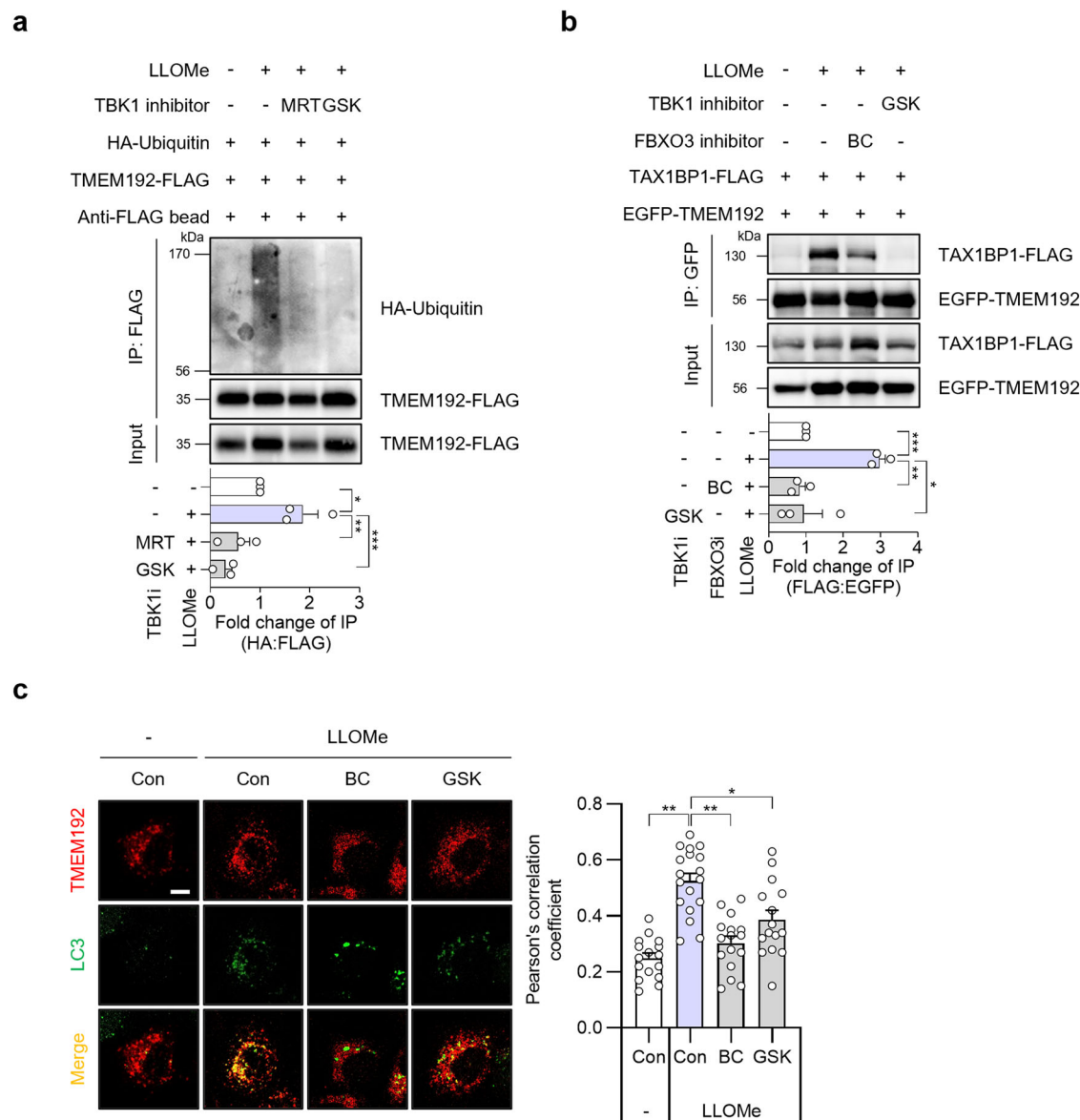


Fig. 5 | Effect of TBK1-FBXO3-TMEM192-TAX1BP1 axis on LLOMe-induced lysophagy. a HepG2 cells were transfected with both HA-ubiquitin and TMEM192-FLAG and pretreated with either MRT67307 (2 μ M) or GSK8612 (10 μ M). LLOMe was cotreated for an additional 2 h. Subsequently, the cells were immunoprecipitated with agarose bead-conjugated anti-FLAG antibody and further analyzed by western blotting using the indicated antibodies. Data are presented as the mean \pm SEM, with each dot in the plot representing independent triplicate replicates of the experiment ($n = 3$, $*p = 0.0446$, $**p = 0.0257$, $***p = 0.0088$). **b** HepG2 cells overexpressing both GFP-TMEM192 and TAX1BP1-FLAG were pretreated with either BC-1215 or GSK8612. LLOMe was cotreated for an additional 2 h. The cells were then pulled down with an anti-GFP antibody conjugated with agarose beads and further

analyzed by western blotting using the indicated antibodies. Data are presented as the mean \pm SEM, with each dot in the plot representing independent triplicate replicates of the experiment ($n = 3$, $*p = 0.0171$, $**p = 0.0006$, $***p = 0.0002$).

c HepG2 cells transiently expressing GFP-LC3 and TMEM192-FLAG were pretreated with either BC-1215 or GSK8612 and cotreated with LLOMe. Subsequently, the cells were stained with an anti-FLAG antibody and imaged by confocal microscopy. The colocalization extent of TMEM192 with LC3 was analyzed using Pearson's correlation coefficients. Data are presented as the mean \pm SEM, with each dot in the plot representing an individual HepG2 cell ($n = 15$, $*p = 0.0031$, $**p < 0.0001$). Scale bar: 10 μ m. All experiments were replicated three times. Two-tailed unpaired t -test were used to analyzed all the data. Source data are provided as a Source Data file.

Methods

Reagents

Bafilomycin A₁ (B1793) and L-leucyl-L-leucine methyl ester (LLOMe, L793) were purchased from Sigma-Aldrich (St. Louis, MO, USA). BC-1215 (HY-117937), GSK8612 (HY-11941) and MRT67307 (HY-13018) were purchased from MedChemExpress (Monmouth Junction, NJ, USA). The short interfering RNA (siRNA) specifically targeting human *ATG5* (5'-CAGGUAAGUCAAGCCUACAUU-3'); *FBXO3* (#1, 5'-CUGUCUAUCACUAUCGUU-3'), (#2, 5'-GAAGAUACAUGACCAUUA-3'); *TMEM192* (#1, 5'-CCAGUAUACACACAGCAAA-3'), (#2, 5'-CUAUUUAAG

CCUAGAAGA-3'); *SQSTM1* (5'-GCAUUGAAGUUGAUUCGAUUU-3'); *TAX1BP1* (#1, 5'-CAAAGAAUUGCUGACAAA-3'), (#2, 5'-CUGGAAUGUCAUACACCUUA-3'), (#3, 5'-AAGAAGAAGTGTAAAGTTAA-3'); *TBK1* (#1, 5'-CCAUGUGGGAGUUUAUACA-3'), (#2, 5'-GCAGUUUGUUUCUCUGUAU-3'); *FBXO2* (#1, 5'-GATGAGAGCGTCAAGAAGT-3'), (#2, 5'-CAGTTCTACTTCTGAGCA-3'); *CUL4A* (#1, 5'-GCACAGAUCCUCCGUUUA-3'), (#2, 5'-GAAGAUUAACACGUGCUGG-3'); *UBE2QL1* (5'-AAGCUGAAGCUACCUUU-3'); and negative scrambled siRNA (5'-CCUACGCCACCAUUUCGU-3') were synthesized by Genolution (Seoul, Korea).

Fig. 6 | Association of FBXO3 with LLOme-induced lysophagy in FBXO3 knockout HepG2 cells. **a** FBXO3 wild-type (WT) and knockout (KO) HepG2 cells were analyzed using western blotting with an FBXO3 antibody. Data are presented as the mean ($n = 2$). **b** FBXO3 WT and KO HepG2 cells expressing GFP-Gal3 were treated with LLOme (2 mM, 3 h), washed, and incubated with fresh medium. The number of GFP-Gal3 puncta per cell was counted. Data are presented as the mean \pm SEM, with each dot representing an individual HepG2 cell ($n = 470$, $^*p < 0.0001$). Scale bar: 10 μ m. **c** FBXO3 WT and KO HepG2 cells expressing HA-ubiquitin and TMEM192-FLAG were treated with LLOme. The cells were immunoprecipitated with anti-TMEM192 antibody and analyzed by western blotting. Data are presented as the mean \pm SEM ($n = 3$, $^*p = 0.0174$, $^{**}p = 0.0011$). **d** FBXO3 WT and KO HepG2 cells expressing EGFP-TMEM192 and TAX1BP1-FLAG were treated with LLOme. Then, the cells were immunoprecipitated with anti-EGFP antibody conjugated with agarose beads and analyzed by western blotting. Data are presented as

the mean ($n = 2$, $^*p = 0.0355$, $^{**}p = 0.0066$). **e** FBXO3 WT and KO HepG2 cells transiently expressing mCherry-Gal3 were reconstituted with empty EGFP, EGFP-FBXO3 WT, or EGFP-FBXO3 V221I. The cells were treated with LLOme, washed, and incubated with fresh culture medium for 24 h. The number of mCherry-Gal3 puncta per cell was counted. Data are presented as the mean \pm SEM, with each dot representing an individual HepG2 cell ($n = 200$, $^*p < 0.0001$). Scale bar: 10 μ m. **f** FBXO3 WT and KO HepG2 cells expressing HA-ubiquitin in combination with empty EGFP, EGFP-FBXO3 WT, or V221I were treated with LLOme. The cells were then immunoprecipitated with anti-TMEM192 antibody and analyzed by western blotting. Data are presented as the mean \pm SEM ($n = 3$, $^*p = 0.0161$, $^{**}p = 0.0039$). All experiments were replicated three times except d (twice replicates). Each dot in the plot **a**, **c**, **d**, and **f** represents independent replicates of the experiment. Two-tailed unpaired *t*-test were used to analyze all the data. Source data are provided as a Source Data file.

create the TMEM192^{K201,211,237,246,254R} and FBXO3^{V221I} mutants, site-directed mutagenesis was performed using the Muta-Directed Mutagenesis Kit (Intron Biotechnology). The specificity of the mutagenesis was confirmed via direct sequencing. The TMEM192 mutant was subcloned into PCR3.1-Flag vector, and the FBXO3 mutant was subcloned onto the pEGFP-C1 vector.

Cell culture and establishment of stable cell lines

HepG2 cells (HB-8065) were purchased from the American Type Culture Collection. To generate stable cell lines, HepG2 cells were transfected with either GFP-Gal3 or CH-Gal3 using Lipofectamine 2000 (Invitrogen, Carlsbad, CA, USA) according to the manufacturer's protocol. Stable transfectants were selected using 1 mg/ml of G418 for 10 days (Invitrogen). After seeding the individual cells, the stable clones were selected under a fluorescence microscope (Olympus, Tokyo, Japan). All cells were cultured at 37 °C in a 5% CO₂ incubator and maintained in Dulbecco's modified Eagle's medium (DMEM; WELGENE, Gyeongsan, Korea) that was supplemented with 10% FBS (WELGENE) and 1% penicillin–streptomycin (WELGENE).

Generation of FBXO3 knockout cell line with CRISPR/Cas9

The FBXO3 knockout HepG2 cell line produced by UBIGENE (Guangzhou, China). CRISPR/Cas9 technology was used to specifically edit the exon 1 region of FBXO3 gene. To target the region, insert oligonucleotides for human FBXO3 (gRNA1R: 5'-AGTCCAAAAAGG ATAAGATGAGG-3'; gRNA2R: 5'-TAGGGTCAGCGCGCCGTCTCGG-3') were annealed and ligated to YKO-RP003 vector (UBIGENE). Then, the YKO-RP003-hFBXO3[gRNA] plasmids containing target sgRNA sequences were transfected onto the HepG2 cells using NeonTM Transfection System (Thermo Fisher Scientific). The transfected cells were selected using puromycin for 2–3 days. After antibiotic selection, the cells were seeded individually. Single FBXO3 KO clones were selected 2–4 weeks later and validated by Sanger sequencing.

Cell-based ubiquitination compound library screening

For the cell-based ubiquitination compound library screening, HepG2/GFP-Gal3 cells were seeded in a 96-well plate. After 24 h, 5–100 μ M of the TargetMol Ubiquitination Compound Library (TargetMol, Wellesley Hills, MA, USA), including 78 ubiquitination-related small molecules targeting proteasomes, the E1/E2/E3 enzymes, DUB and p97, was cotreated with LLOme to each well. GFP-Gal3 puncta in the cells were monitored via fluorescence microscopy (Olympus) and Operetta CLSTM High-content analysis system (Perkin Elmer, MA, USA). The experiments were performed in triplicate.

Western blotting

For immunoblotting, the cells were lysed using a cell lysis buffer, with 2x Laemmli sample buffer added to the lysate (Bio-Rad, Hercules, CA, USA). The total protein was quantified using the Bradford solution (Bio-Rad) according to the manufacturer's instructions. The samples were

separated by SDS-PAGE and transferred to a PVDF membrane (Bio-Rad). After blocking with 4% skim milk (MBcell, Seoul, Korea) in TBST (25 mM Tris-base, 140 mM NaCl, and 0.05% Tween[®] 20 [Sigma-Aldrich]), the membrane was probed with the following primary antibodies: anti-LC3 (NB100-2220, 1:3000), purchased from NOVUS Biologicals (Centennial, CO, USA); anti-FLAG (2368, 1:3000), anti-p-TBK1 Ser172 (5483, 1:1000), anti-TBK1 (3013, 1:1000) and anti-SQSTM1 (5114, 1:1000) antibodies purchased from Cell Signaling Technology (Danvers, MA, USA); anti-GFP (sc-9996; 1:1000), anti-FBXO3 (sc-514625, 1:1000), and anti-HA (sc-7392, 1:1000) antibodies purchased from Santa Cruz Biotechnology (Dallas, TX, USA); anti-TMEM192 (28263-1-AP, 1:3000) and anti-TAX1BP1 (14424-1-AP, 1:1000) antibodies purchased from Proteintech (Rosemont, IL, USA); anti- α -ACTIN (ACTA1, MAB1501, 1:10,000) and anti-FLAG (F18804-1MG, 1:3000) antibodies purchased from Sigma-Aldrich. The membranes were incubated with HRP-conjugated secondary antibodies (Cell Signaling Technology). The signals were detected using Luminograph I (ATTO, Tokyo, Japan).

Immunoprecipitation

For the immunoprecipitation assay, cells were homogenized in a RIPA buffer (50 mM Tris-HCl, pH 7.5, 150 mM sodium chloride, 0.5% sodium deoxycholate, 1% Triton X-100, 0.1% SDS and 2 mM EDTA; Intron Biotechnology, Seoul, Korea) containing protease inhibitors (GenDEPOT) for 1 h at 4 °C. For the exogenous IP assays, the supernatant was immunoprecipitated with the following antibodies: anti-GFP-agarose (sc-9996 AC, 3 μ g) and anti-HA-agarose antibodies (sc-7392 AC, 3 μ g) acquired from Santa Cruz Biotechnology; and anti-FLAG-agarose antibodies (ab1240, 1.5 μ g) obtained from Abcam. For the endogenous IP assay, the supernatant was immunoprecipitated with the following antibodies: anti-FBXO3 antibodies (sc-514625, 3 μ g) obtained from Santa Cruz Biotechnology; and anti-TMEM192 antibodies (28263-1-AP, 3 μ g) acquired from Proteintech with a protein G plus/protein A agarose suspension (Santa Cruz Biotechnology, sc-2003) overnight at 4 °C. After incubation, the samples were washed with a RIPA buffer twice at 4 °C and added with 2x Laemmli sample buffer (Bio-Rad). All samples were analyzed by western blotting as described in the western blotting section.

Phos-tagTM SDS-PAGE

For Phos-tagTM SDS-PAGE, Phos-tagTM Acrylamide (Wako, Osaka, Japan) with Mn²⁺ was used. Phos-tag Acrylamide (35 μ M) and MnCl₂ (7 μ M) were added to the separating gel before polymerization. Electrophoresis was performed (25 mA/gel) under constant-current conditions. After electrophoresis, the gel was gently washed four times with transfer buffer containing 10 mM EDTA for 20 min each. After washing, the gel was immersed in the transfer buffer without EDTA for 20 min and transferred to PVDF membrane (Bio-Rad).

Fluorescence microscopy

Cells were treated with various chemicals or siRNA and fixed with 4% paraformaldehyde for 10 min. Samples were then observed using a

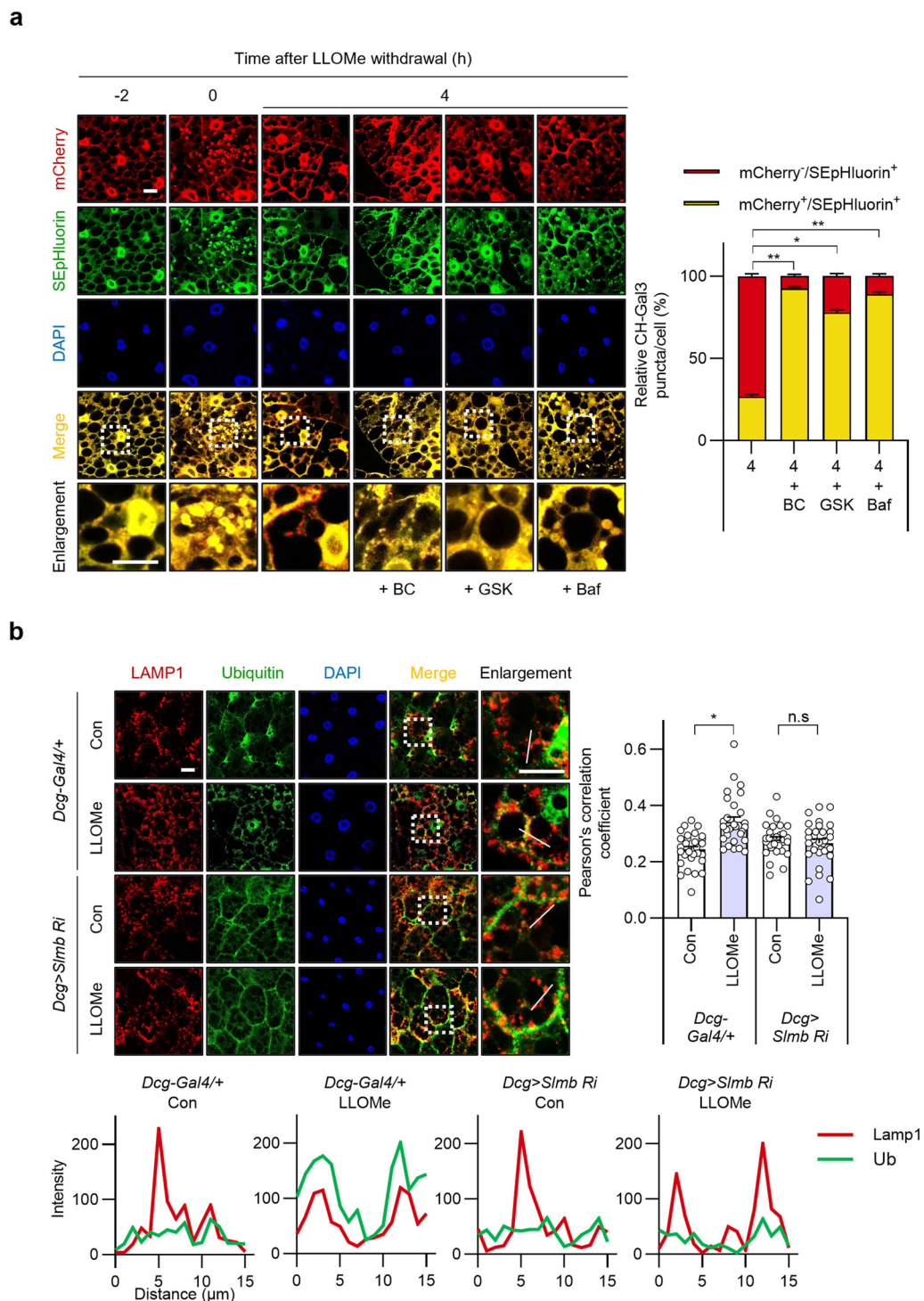


Fig. 7 | Association of TBK1-FBXO3-TMEM192-TAX1BP1 axis with LLOMe-induced lysophagy in *Drosophila* model. **a** Cotreatment of Baf, BC-1215, or GSK612 with LLOMe showed decrease of mCherry⁺/SEpHluorin⁺ Gal3 puncta in larva fat body. The number of mCherry/SEpHluorin puncta per cell was quantified. Data are presented as the mean \pm SEM ($n = 150$, $*p = 0.0003$, $**p < 0.0001$). A total of 150 individual larva fat body cells were counted. Scale bar: 20 μm . **b** Feeding third-instar larvae of control (*Dcg-Gal4/+*) and *Slmb* knockdown (*Dcg>Slmb Ri*) flies were fed with normal fly food containing LLOMe. After a 2-h feeding period, larvae in the

wandering stage were dissected, costained with anti-ubiquitin and anti-LAMP1 antibodies, and subsequently imaged using confocal microscopy. The colocalization of LAMP1 and ubiquitin staining was analyzed by Pearson's correlation coefficient and line colocalization. The fluorescence intensities of both LAMP1 and Ubiquitin were quantified. Data are presented as the mean \pm SEM, with each dot in the plot representing an individual fat body cell ($n = 30$, $*p < 0.0001$). Scale bar: 20 μm . All experiments were replicated three times. Two-tailed unpaired *t*-test were used to analyze all the data. Source data are provided as a Source Data file.

fluorescence microscope (Olympus). The number of Gal3 puncta was analyzed using Image J software (NIH, Bethesda, MD, USA). The data analyses were performed using GraphPad Prism 10 (GraphPad Software, San Diego, CA, USA).

Identification of lysophagic cells

To quantify cells with lysophagy, HepG2/CH-Gal3 cells were cotreated with LLOMe and either Baf or BC-1215 for 2 h. Afterward, LLOMe was washed out with fresh medium and incubated with either Baf or

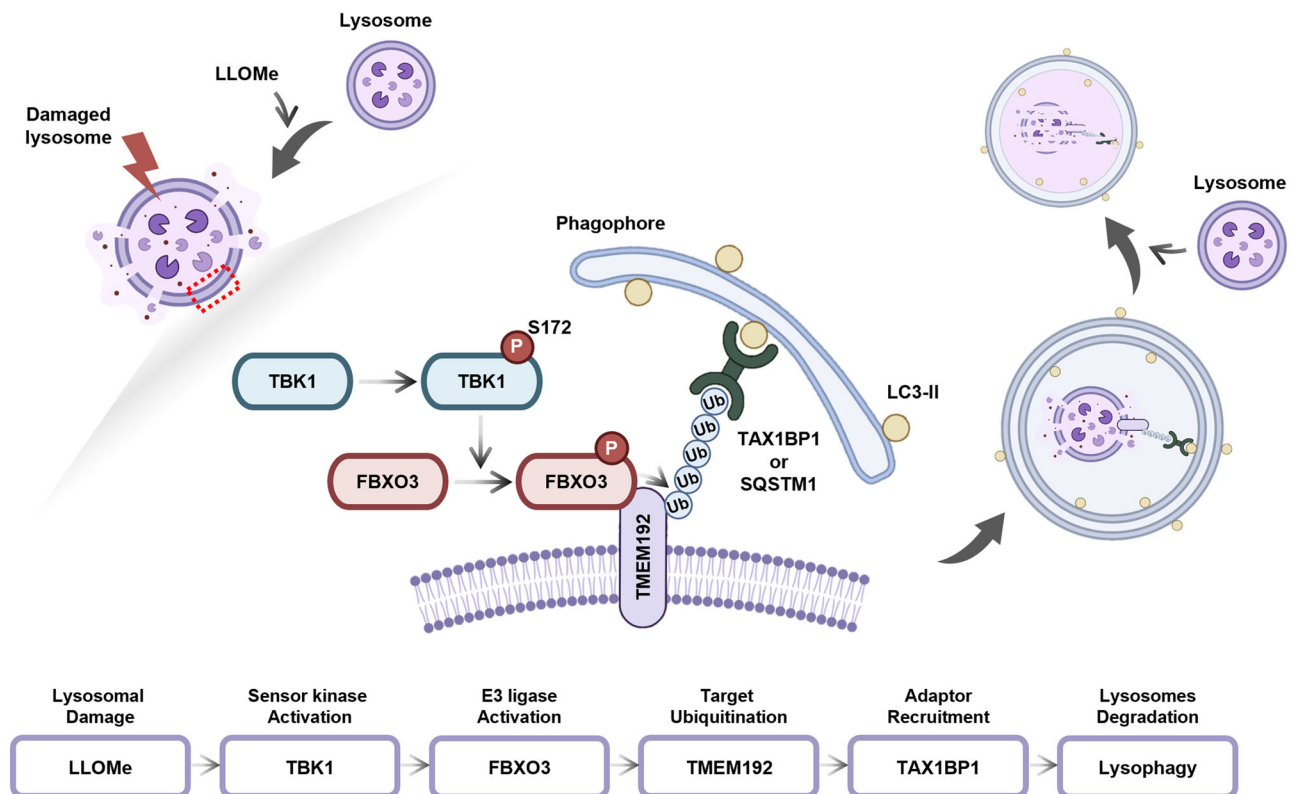


Fig. 8 | Schematic diagram of a lysophagy regulatory mechanism by TBK1-FBXO3-TMEM192-TAX1BP1 axis. Lysosomotropic agents, such as LLOMe, induce lysosomal damage. With severe damage, the ruptured lysosomes are degraded by lysosome selective autophagy, lysophagy. In response to lysosomal rupture, TBK1 is activated via phosphorylation on S172 and mediates phosphorylation of FBXO3, a

component of SCF E3 ligase complex. Subsequently, the FBXO3 mediates ubiquitination of lysosomal membrane protein TMEM192. This ubiquitination promotes the recruitment of autophagy adaptor protein SQSTM1 or TAX1BP1 and other autophagic machineries, leading to the degradation of damaged lysosomes. Some icons were created in BioRender. Jo, D. (2025) <https://BioRender.com/g56j185>.

BC-1215 for 24 h. The fluorescence images were obtained using a fluorescence microscope (Olympus). The number of mCherry- and SEpHluorin-double-positive-Gal3 puncta (mCherry⁺/SEpHluorin⁺) and mCherry-positive/SEpHluorin-negative-Gal3 puncta (mCherry⁺/SEpHluorin⁻) were counted using Image J (NIH). The obtained data were analyzed using GraphPad Prism 10.

Confocal microscopy

HepG2 cells were grown on a cover-glass and cotransfected with the plasmids. For colocalization studies, cells were transfected with pTMEM192-FLAG in combination with either pEGFP-SQSTM1 or pTAX1BP1-EGFP, or with pEGFP-TMEM192 and either mCherry-NBR1 or pOPTN-EGFP. After 24 h, the cells were treated with LLOMe for another 2 h. Next, the cells were washed with phosphate-buffered saline (PBS) and fixed with 4% paraformaldehyde for 20 min. For permeabilization, the cells were incubated with 0.1% Triton X-100 for 2 min and blocked with 2% BSA in PBS for 1 h at RT. After blocking, the cells were incubated with anti-FLAG antibodies (Sigma-Aldrich) overnight. The cells were then washed with PBS and incubated with Alexa Fluor 555 Goat anti-mouse IgG antibodies (Thermo Fisher, Waltham, MA, USA) overnight. The fluorescence images of TMEM192 colocalized with TAX1BP1 were obtained using a confocal laser scanning microscope (Carl Zeiss, LSM 800).

Drosophila genetics

All *Drosophila* strains were grown and maintained at 25 °C. The following *Drosophila* strains were used: *DcG-Gal4* (a gift from Dr. K. Yu, KRIBB, Korea), *UAS-slm RNAi* (# 31056, Bloomington Drosophila Stock Center) (Bloomington, IN, USA). For generation of UAS-mCherry-SEpHluorin-Gal3, cDNA sequence of mCherry-SEpHluorin-

Gal3 was cloned into the pUAST vector. We used the microinjection service provided by Korea Drosophila Resource Center (KDRC, Korea) to create a UAS-mCherry-SEpHluorin-Gal3 transgenic fly with the transgene inserted on the second chromosome.

Drosophila LLOMe treatment

To induce lysophagy in *Drosophila*, LLOMe was administered in standard food at a concentration of 5 mM. The inhibitor treatments in LLOMe-containing food included BC-1215 (5 mM), Baf (15 μM) and GSK8612 (1 mM). All the mentioned treatments were dissolved in 99.9% ethanol. For the lysophagy experiments, third-instar stage larvae were first washed in PBS to eliminate any residual food and then transferred to food containing LLOMe. After a 2-h exposure, larvae were either immediately dissected or transferred to normal/inhibitor-containing food for specific time intervals.

Drosophila immunostaining

Larval fat body tissues were dissected in 1X PBS, fixed for 20 min in 4% paraformaldehyde, and washed 3 times with PBS. After fixation, tissues were blocked for 30 min with blocking solution (1X PBS, 0.1% Triton X-100, 4% BSA) in room temperature. Then, tissues were incubated in antibody solution overnight at 4 °C and washed six times with PBST (1X PBS, 0.1% Triton X-100). Next, tissues were incubated in secondary antibody solution overnight at 4 °C (or room temperature for 2 h). The tissues were mounted in the Vectashield Antifade Mounting Medium with DAPI (H-1200-10, Vector Laboratories, USA) and fluorescence images were acquired by the confocal Microscope (Leica, STELLARIS 5, Germany). The following primary and secondary antibodies were used: rabbit anti-Lamp1 (1:200, NY2403, a gift from Dr. Andreas Jenny), anti-ubiquitinated proteins

clone FK2 (1:200, Sigma-Aldrich, 04-263), IgG anti-rabbit IgG Alexa 488 (1:500, Bioacts, Korea) were used.

Statistical analysis

Data were obtained from at least three independent experiments and presented as means \pm SEM. All statistical analyses were performed using GraphPad Prism 10 software. The results were statistically evaluated using two-tailed unpaired *t*-test. Differences of $P < 0.05$ were considered significant.

Reporting summary

Further information on research design is available in the Nature Portfolio Reporting Summary linked to this article.

Data availability

The main data supporting the findings of this study are available within the article and its Supplementary information. The source data for all figures in this paper are provided in the accompanying Source data file. Source data are provided with this paper.

References

- Settembre, C., Fraldi, A., Medina, D. L. & Ballabio, A. Signals from the lysosome: a control centre for cellular clearance and energy metabolism. *Nat. Rev. Mol. Cell Biol.* **14**, 283–296 (2013).
- Saftig, P. & Puertollano, R. How lysosomes sense, integrate, and cope with stress. *Trends Biochem. Sci.* **46**, 97–112 (2021).
- Zoncu, R. & Perera, R. M. Built to last: lysosome remodeling and repair in health and disease. *Trends Cell Biol.* **32**, 597–610 (2022).
- Saftig, P. & Klumperman, J. Lysosome biogenesis and lysosomal membrane proteins: trafficking meets function. *Nat. Rev. Mol. Cell Biol.* **10**, 623–635 (2009).
- Allemaille, K. S. et al. Novel approaches of dysregulating lysosome functions in cancer cells by specific drugs and its nano-formulations: a smart approach of modern therapeutics. *Int. J. Nanomed.* **16**, 5065–5098 (2021).
- Perera, R. M. & Zoncu, R. The lysosome as a regulatory hub. *Annu. Rev. Cell. Dev. Biol.* **32**, 223–253 (2016).
- Machado, E. R., Annunziata, I., van de Vlekkert, D., Grosveld, G. C. & d'Azzo, A. Lysosomes and cancer progression: a malignant liaison. *Front. Cell Dev. Biol.* **9**, 642494 (2021).
- Trivedi, P. C., Bartlett, J. J. & Pulinkunnil, T. Lysosomal biology and function: modern view of cellular debris bin. *Cells* **9**, 1131 (2020).
- Maejima, I. et al. Autophagy sequesters damaged lysosomes to control lysosomal biogenesis and kidney injury. *EMBO J.* **32**, 2336–2347 (2013).
- Park, N. Y. et al. Triamterene induces autophagic degradation of lysosome by exacerbating lysosomal integrity. *Arch. Pharm. Res.* **44**, 621–631 (2021).
- Halle, A. et al. The NALP3 inflammasome is involved in the innate immune response to amyloid-beta. *Nat. Immunol.* **9**, 857–865 (2008).
- Wang, F., Gomez-Sintes, R. & Boya, P. Lysosomal membrane permeabilization and cell death. *Traffic* **19**, 918–931 (2018).
- Boya, P. Lysosomal function and dysfunction: mechanism and disease. *Antioxid. Redox Signal.* **17**, 766–774 (2012).
- Radulovic, M. et al. ESCRT-mediated lysosome repair precedes lysophagy and promotes cell survival. *EMBO J.* **37**, e99753 (2018).
- Medina, D. L. et al. Lysosomal calcium signalling regulates autophagy through calcineurin and TFEB. *Nat. Cell Biol.* **17**, 288–299 (2015).
- Sardiello, M. et al. A gene network regulating lysosomal biogenesis and function. *Science* **325**, 473–477 (2009).
- Stolz, A., Ernst, A. & Dikic, I. Cargo recognition and trafficking in selective autophagy. *Nat. Cell Biol.* **16**, 495–501 (2014).
- Johannes, L., Jacob, R. & Leffler, H. Galectins at a glance. *J. Cell Sci.* **131**, jcs208884 (2018).
- Winchester, B. G. Lysosomal membrane proteins. *Eur. J. Paediatr. Neurol.* **5**, 11–19 (2001).
- Schwake, M., Schroder, B. & Saftig, P. Lysosomal membrane proteins and their central role in physiology. *Traffic* **14**, 739–748 (2013).
- Aits, S. et al. Sensitive detection of lysosomal membrane permeabilization by lysosomal galectin puncta assay. *Autophagy* **11**, 1408–1424 (2015).
- Aits, S. Methods to detect loss of lysosomal membrane integrity. *Methods Mol. Biol.* **1880**, 315–329 (2019).
- Otomo, T. & Yoshimori, T. Lysophagy: a method for monitoring lysosomal rupture followed by autophagy-dependent recovery. *Methods Mol. Biol.* **1594**, 141–149 (2017).
- Jia, J. et al. Galectin-3 coordinates a cellular system for lysosomal repair and removal. *Dev. Cell* **52**, 69–87.e68 (2020).
- Yoshida, Y. et al. Ubiquitination of exposed glycoproteins by SCF(FBXO27) directs damaged lysosomes for autophagy. *Proc. Natl Acad. Sci. USA* **114**, 8574–8579 (2017).
- Teranishi, H. et al. Identification of CUL4A-DDB1-WDFY1 as an E3 ubiquitin ligase complex involved in initiation of lysophagy. *Cell Rep.* **40**, 111349 (2022).
- Koerver, L. et al. The ubiquitin-conjugating enzyme UBE2QL1 coordinates lysophagy in response to endolysosomal damage. *EMBO Rep.* **20**, e48014 (2019).
- Eapen, V. V., Swarup, S., Hoyer, M. J., Paulo, J. A. & Harper, J. W. Quantitative proteomics reveals the selectivity of ubiquitin-binding autophagy receptors in the turnover of damaged lysosomes by lysophagy. *eLife* **10**, e72328 (2021).
- Thurston, T. L., Wandel, M. P., von Muhlinen, N., Foeglein, A. & Randow, F. Galectin 8 targets damaged vesicles for autophagy to defend cells against bacterial invasion. *Nature* **482**, 414–418 (2012).
- Choubey, V., Zeb, A. & Kaasik, A. Molecular mechanisms and regulation of mammalian mitophagy. *Cells* **11**, 38 (2021).
- Kane, L. A. et al. PINK1 phosphorylates ubiquitin to activate Parkin E3 ubiquitin ligase activity. *J. Cell Biol.* **205**, 143–153 (2014).
- Lazarou, M. et al. The ubiquitin kinase PINK1 recruits autophagy receptors to induce mitophagy. *Nature* **524**, 309–314 (2015).
- Chen, B. B. et al. A combinatorial F box protein directed pathway controls TRAF adaptor stability to regulate inflammation. *Nat. Immunol.* **14**, 470–479 (2013).
- Hung, K. Y. et al. Targeting F-box protein Fbxo3 attenuates lung injury induced by ischemia-reperfusion in rats. *Front. Pharmacol.* **10**, 583 (2019).
- Liu, E. A. et al. Fbxo2 mediates clearance of damaged lysosomes and modifies neurodegeneration in the Niemann-Pick C brain. *JCI Insight* **5**, e136676 (2020).
- Krzysiak, T. C., Chen, B. B., Lear, T., Mallampalli, R. K. & Gronenborn, A. M. Crystal structure and interaction studies of the human Fbxo3 ApaG domain. *FEBS J.* **283**, 2091–2101 (2016).
- Abu-Remaileh, M. et al. Lysosomal metabolomics reveals V-ATPase- and mTOR-dependent regulation of amino acid efflux from lysosomes. *Science* **358**, 807–813 (2017).
- Schroder, B., Wrocklage, C., Hasilik, A. & Saftig, P. Molecular characterisation of 'transmembrane protein 192' (TMEM192), a novel protein of the lysosomal membrane. *Biol. Chem.* **391**, 695–704 (2010).
- Pied, N. et al. TBK1 is part of a galectin 8 dependent membrane damage recognition complex and drives autophagy upon Adenovirus endosomal escape. *PLoS Pathog.* **18**, e1010736 (2022).
- Seth, P. Mechanism of adenovirus-mediated endosome lysis: role of the intact adenovirus capsid structure. *Biochem. Biophys. Res. Commun.* **205**, 1318–1324 (1994).
- Wang, W. H. et al. The role of galectins in virus infection - A systemic literature review. *J. Microbiol. Immunol. Infect.* **53**, 925–935 (2020).
- Xie, J., Jin, Y. & Wang, G. The role of SCF ubiquitin-ligase complex at the beginning of life. *Reprod. Biol. Endocrinol.* **17**, 101 (2019).

43. Thompson, L. L., Rutherford, K. A., Lepage, C. C. & McManus, K. J. The SCF complex is essential to maintain genome and chromosome stability. *Int. J. Mol. Sci.* **22**, 8544 (2021).
44. Zhang, Z. et al. Diverse roles of F-BoxProtein3 in regulation of various cellular functions. *Front. Cell Dev. Biol.* **9**, 802204 (2022).
45. Granger, B. L. et al. Characterization and cloning of lgp110, a lysosomal membrane glycoprotein from mouse and rat cells. *J. Biol. Chem.* **265**, 12036–12043 (1990).
46. Ohashi, S. et al. Comparative analysis of site-specific N-glycosylation of LAMP1 from breast cancer tissues. *J. Biochem.* **175**, 561–572 (2024).
47. Nguyen, T. L. et al. Functional characterization of the lysosomal membrane protein TMEM192 in mice. *Oncotarget* **8**, 43635–43652 (2017).
48. Cardozo, T. & Pagano, M. The SCF ubiquitin ligase: insights into a molecular machine. *Nat. Rev. Mol. Cell Biol.* **5**, 739–751 (2004).
49. Smelkinson, M. G. & Kalderon, D. Processing of the Drosophila hedgehog signaling effector Ci-155 to the repressor Ci-75 is mediated by direct binding to the SCF component Slimb. *Curr. Biol.* **16**, 110–116 (2006).
50. Zhang, H. et al. SCF(Slimb) E3 ligase-mediated degradation of expanded is inhibited by the Hippo pathway in Drosophila. *Cell Res.* **25**, 93–109 (2015).

Acknowledgements

We thank Dr. Zhi-Xiong Jim Xiao (Sichuan University, China) for providing the HA-FBXO3 plasmids, including the wild-type (WT), domain deletion mutants (Δ F-box, Δ SUKH, Δ ApaG) and point mutants (S26A, S166A, S356A, and T82A). D.-H.C. was supported by the National Research Foundation of Korea, funded by the Ministry of Science & ICT [RS-2024-00338475], and by Korea Institute for Advancement of Technology funded by the Ministry of Trade, Industry and Energy [P0025489]. N.Y.P. was supported by Basic Science Research Program through the National Research Foundation of Korea (NRF) funded by the Ministry of Education [RS-2024-00453488 and RS-2024-00463344]. J.-E.B. was supported by Basic Science Research Program through the National Research Foundation of Korea (NRF) funded by the Ministry of Education [RS-2024-00463344]. E.Y. was supported by G-LAMP Program of the National Research Foundation of Korea (NRF) grant funded by the Ministry of Education [RS-2023-00301914]. This research was also supported by the ORGASIS Corporation.

Author contributions

N.Y.P., D.S.J., and D.-H.C. designed the research study; N.Y.P., D.S.J., and J.-Y.Y. performed the cell experiments and animal experiments; N.Y.P. analyzed and interpreted the results and designed the figures; N.Y.P., E.Y.

and D.-H.C. contributed to writing original draft preparation; N.Y.P., D.S.J., J.-E.B., J.B.K., Y.H.K., S.H.K., E.Y., and D.-H.C. performed review and editing; D.-S.L., T.Y., and E.-K.J. contributed to conceptualization and review the manuscript; D.-H.C. performed project administration; P.S.K. and D.-H.C. acquired funding acquisition; E.Y. and D.-H.C. performed supervision; all the authors contributed to editorial changes and approved the final manuscript.

Competing interests

The authors declare no competing interests.

Additional information

Supplementary information The online version contains supplementary material available at <https://doi.org/10.1038/s41467-025-56294-y>.

Correspondence and requests for materials should be addressed to Eunbyul Yeom or Dong-Hyung Cho.

Peer review information *Nature Communications* thanks Jingyue Jia and the other, anonymous, reviewer(s) for their contribution to the peer review of this work. A peer review file is available.

Reprints and permissions information is available at <http://www.nature.com/reprints>

Publisher's note Springer Nature remains neutral with regard to jurisdictional claims in published maps and institutional affiliations.

Open Access This article is licensed under a Creative Commons Attribution-NonCommercial-NoDerivatives 4.0 International License, which permits any non-commercial use, sharing, distribution and reproduction in any medium or format, as long as you give appropriate credit to the original author(s) and the source, provide a link to the Creative Commons licence, and indicate if you modified the licensed material. You do not have permission under this licence to share adapted material derived from this article or parts of it. The images or other third party material in this article are included in the article's Creative Commons licence, unless indicated otherwise in a credit line to the material. If material is not included in the article's Creative Commons licence and your intended use is not permitted by statutory regulation or exceeds the permitted use, you will need to obtain permission directly from the copyright holder. To view a copy of this licence, visit <http://creativecommons.org/licenses/by-nc-nd/4.0/>.

© The Author(s) 2025